Image deconvolution as an aid to mammographic artefact identification I:basic techniques

P. Abbott[a], A. Shearer[a], T O'Doherty[a] and W. van der Putten[b]

[a]Information Technology Centre, National University of Ireland, Galway,Ireland

[b]Medical Physics, University College Hospital, Galway, Ireland

ABSTRACT

Digital mammography has the potential to provide radiologists with a tool which can detect tumours earlier and with greater accuracy then film based systems. Although a digital mammography system can provide much greater contrast when compared with a conventional film system, the ability to detect small artifacts associated with breast cancer is limited by a reduced spatial resolution due to screen unsharpness and scatter induced fog. In this paper we model the radiological image formation process as the convolution of a linear shift invariant point spread function (PSF) with the projected tissue density source function. We model the PSF as consisting of two components - screen unsharpness and scatter. We present results from a method designed to compensate for screen unsharpness. The screen PSF was measured and subsequently used in an iterative deconvolution algorithm which incorporated wavelet based de-noising between steps in order to reduce noise amplification. When applied to a University of Leeds TORMAX breast phantom the results show as much as a two-fold improvement in resolution at the 50 percent MTF level. Our results show that the regularized deconvolution algorithm significantly improves the signal-to-noise ratio in the restored image.

Keywords: Mammography,Deconvolution,Wavelet Denoising

1. INTRODUCTION

Among women, breast cancer accounts for one third of all cancers detected and 18 percent of all cancer deaths. Until recently breast cancer was the leading cause of death among women but since 1985 it has ranked second to lung cancer. Prevention of this disease is difficult since its cause is not fully understood. Current methods of treatment are very effective against breast cancer in its early phase.[1] Therefore, the most promising way to achieve a change in the current breast cancer situation is to remove the cancer in its early stages. Although the early detection of breast cancer is most reliably achieved with mammography, there exists a significant number of false-negative cases.[2] These may be attributed in part to a failure by the radiologist and it has been suggested that a second radiologist be used in mass screening programmes to lower the false-negative rate. Using a second radiologist would be prohibitive in terms of labour costs - consequently it has been suggested that an automated computer screening programme be used for this purpose. Obviously the ability of any automatic procedure is determined by resolution of the underlying image. There are three main difficulties with the analysis of mammograms by computer. Firstly, it involves the analysis of small features of low contrast superimposed onto non-uniform backgrounds. Locating suspicious areas (i.e. tumour symptoms) in mammograms is difficult. There is little difference in density between normal and tumerous tissue in human breasts and so the contrast between a tumour area and it's background in the image is minimal. This contrast is further reduced in the filming and digitisation process of the mammogram images. Also the background of the tumour area is increased by noise and anatomical structures, such as ducts and glands. Early stage tumours are very small so all these factors contribute to the difficulty of detection of tumours in mammograms. Secondly, the diagnostic information content in the mammograms is more interpretative than statistical in nature.[3] That is, the features essential for diagnosing a particular disease are determined both by the disease and the class of the image. Thirdly, the resolution required in a particular disease application may, for example, be an order of magnitude higher than that necessary for all general diseases using the same class of image. The radiographic signs of carcinoma include masses, calcifications, areas of asymmetric densities or distortion of architecture, prominent lactiferous ducts and skin or nipple thickening and/or retraction.[4] It has been reported that 30% to 50% of breast carcinomas detected mammographically demonstrate clustered micro-calcifications,[5] although about 80% of breast carcinomas reveal

Address correspondence to A.Shearer : E-mail: shearer@itc.nuigalway.ie

Figure 1. Simplified xray imaging device

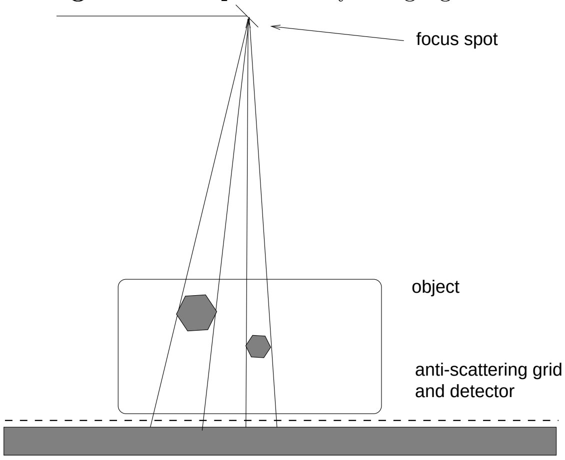

micro-calcifications on microscopic examination.[6] In addition studies indicate that 26% of cancers which are not obvious from touch appear mammographically as a mass and 18% appear with both a mass and micro-calcifications.[7] Computational methods are being developed for the specific detection of either mass lesions or micro-calcifications. This detection takes place in two steps. Firstly a pre-processing step is carried out in which the whole image is enhanced.. Then the individual tumours are detected using different methods which include segmenting the tumours from the image and applying a specific mathematical method to accurately detect the position and size of the tumour. This paper concentrates upon the first stage and investigates the use of image restoration in digital mammography.

2. RADIOGRAPHIC IMAGE FORMATION AND DECONVOLUTION

A radiographic image measures the intensity of x-ray radiation transmitted through an object. In medical imaging the difference in attenuation between tissue types such as bone and muscle results in contrast. It is thus contrast which carries information in a medical radiographic image. In this section we review the basics of radiographic image formation and the physical mechanisms which lead to reduction in contrast. We then propose a computational method by which the contrast may be improved.

Figure 1 shows a simplified x-ray imaging device. X-ray photons emitted from the anode pass through the object of interest, are absorbed or scattered in the object and the resulting intensity is measured at the imaging plane. As with any imaging system there are constraints on the resolution of the measured image. In radiographic imaging there are several sources of image degradation including focus spot,scatter and screen unsharpness. In order to model image degradation we write the image formation equation in the usual way

$$I(x,y) = O(x,y) * P(x,y) + N(x,y)\,, \tag{1}$$

where $I(x,y)$ is the measured intensity, $O(x,y)$ is the object, $P(x,y)$ is the point spread function (PSF) and $N(x,y)$ is noise. Since we are measuring xray attenuation we may consider $O(x,y)$ to be the distribution of electron density. The contribution to the PSF from a finite focus spot may be found by considering the impulse response. Consider a pinhole placed a distance D from the focus spot and d above the image plane. The response is an image of the focus spot, with a magnification given by d/D. In a typical mammography setup with d = 5cm, D = 55cm and a focus spot of 300 microns, this would result in a measured focus spot of approximately 30 microns or approximately 0.3 of a pixel for a digital system with 9 pixels/mm. We can therefore neglect the effect of a finite focus spot when we have the object sufficiently close to the imaging plane, ie when magnification is not being used. Also of interest is the distribution of xray intensity across the anode, which is not in general uniform.

In radiological imaging we can classify xray photons arriving at the detector into two catagorys - primary photons which do not interact with the object and scattered photons - those that have interacted with the object via coherent or incoherent scattering.[8] It is the primary photons which carry information - scattered photons do not contribute to the information content in the first order, instead they act to decrease the contrast of high frequency features and regions of low contrast. In a companion paper[9] we investigate a method for measurement and correction of the scatter component of extended PSF due to scatter.

Our focus in this paper is the correction of degradation due to screen unsharpness - the instrumental component pf the PSF. Digital radiography systems presently in use are based upon light conversion technology. As with a traditional film/screen system a phosphor screen is used to convert incident xray photons into visible light to create an optical image. This is then recorded using a photo-electric detector such as a CCD or photodiode array. The resolving power of these systems is limited by scattering visible light within the phosphor screen, and additionally by the light coupling stage.[10]

In addition to the blurring of the object due to the PSF the other source of image degradation is noise. In digital radiography this arises both from the statistical nature of x-ray emission and from noise introduced in the light coupling stage. The measurement of xray intensity is a counting process and hence subject to Poisson noise.

2.1. Image Restoration

The process of recovering or estimating the object image $O(x, y)$ from an observed image $I(x, y)$ in Eq. 1 is a well studied problem in image processing. When the PSF $P(x, y)$ is unknown the problem is referred to as blind deconvolution. In our case however we assume that the PSF is known. The process of recovering $O(x, y)$ then becomes an inverse problem. Although it is possible to find the inverse of Eq. 1 by Fourier transform, the result is not satisfactory due to amplification of high frequency noise.

This type of inverse problem related to image restoration has been the subject of much research in astronomy, where the PSF is due to instrumental response combined with atmospheric effects (*seeing*). The approach adopted by Lucy[11] derives from Bayes theorem. The solution given by Eq. 2 effectively finds an estimate $\psi(x, y)$ that maximizes the likelihood of the observed image $I(x, y)$ at each iteration. The nth estimate $\psi_n(x, y)$ is given by

$$\psi_n(x,y) = \psi_{n-1}(x,y) \left[\frac{I(x,y)}{\psi_{n-1}(x,y) * P(x,y)}\right] * P(-x,-y)\,. \tag{2}$$

The success of Eq. 2 in astronomical image restoration is due in part to the ability to accurately measure the PSF Likewise the success of this technique in restoration of radiographic images will be determined by the accuracy to which the PSF is measured.

2.2. Regularized Deconvolution

In practice the image restoration algorithm described above suffers from amplification of noise as the number of iterations is increased. At a high enough number of iterations the image begins to break down. In effect noise present in the original image is mistaken for high frequency features. In order to overcome this limitation Starck et al[12] have proposed a regularization technique based on a wavelet denoising algorithm applied to the residual between iterations. The residual is defined as

$$R^{(n)}(x,y) = I(x,y) - P(x,y) * O^{(n)}(x,y) \tag{3}$$

where $O^{(n)}(x, y)$ is the object estimate at the nth iteration. Specifically the algorithm performs a hard threshold of the wavelet coefficients of the residual. The threshold level is set by a study of variation of Gaussian noise in this wavelet space. Although the algorithm proposed by[12] is effective, it is computationally demanding due to the redundant a'trous wavelet transform applied. In addition the method used to set the denoising threshold is based on the assumption of Gaussian noise. In order to improve upon this we have developed an algorithm based on a non-redundant transform - the Daubechies wavelet[13] which is more efficient in terms of storage. We denoise the residual between iterations by using a soft thresholding (wavelet shrinkage) which is statistically more attractive then hard thresholding.[14] We select the level dependent soft threshold as a fraction k of the wavelet coefficient standard deviation.

3. METHOD

In order to accurately measure the PSF many point sources are required.[15] In astronomy this is easily done because stars are regarded as point sources since the angular diameter of the largest star is always less than the instrumental/seeing PSF. A typical radiographic image does not contain such features naturally within it. To overcome this problem we have designed a mask to provide point sources from which the PSF may be calculated.

Each mask consists of a thin sheet of steel containing 20 holes arranged in a 4x5 grid. Assuming no magnification, that is when the mask is sufficiently close to the detector, these holes may be regarded as point sources if the diameter is less then the resolution of the detector. In our work we used a Siemens Mammomat 3 with Agfa Computed Radiography phosphor plates digitised on an Agfa ADC readout unit. We used holes with a 100 micron diameter, which we may assume is sufficiently less than the detector resolution which is sampled at 110 microns per pixel (9 pixels per millimetre). Although it is possible to use smaller diameter holes we found that 100 micron diameter holes provided an adequate point source with an acceptable signal-to-noise (SNR). As discussed scatter and noise are important factors contributing to the PSF formation. To simulate scatter in the breast we use a phantom which is made from perspex. Perspex is a tissue equivalent material so a height of perspex block represents the same thickness of a compressed breast. An average compressed breast has a thickness of 4.5cm, consequently we used a 4.5cm thick perspex block.

In order to improve the SNR of the measured PSF we add the response from a number of point sources together. Four masks were placed side by side within the perspex phantom. Five images were taken of this setup. The masks were randomly shifted with respect to the instrument for each image but were not shifted relative to each other. Each digitised image was then registered, that is, aligned relative to the first image taken. The five registered images were then added together. To alleviate edge effects only the 8 central holes on each grid were identified and added together. In all, 160 holes were used to create the measured PSF.

4. RESULTS

In order to quantify the improvement in resolution we used a breast phantom card (TORMAX, University of Leeds) containing embedded resolution and contrast targets. The phantom is shown before restoration in Fig. 2. The modulation transfer function (MTF) for the horizontal resolution chart was used to assess the restoration algorithm. In order to find the MTF each of the three line groups was column averaged. The intensity was then plotted and the MTF calculated as

$$MTF = (I_1 - I_2)/(I_2 + I_1) \tag{4}$$

where I_1 is the intensity of the peak and I_2 is the intensity of the trough. Each spatial frequency group consists of 4.5 cycles of a square wave. The MTF was calculated only when each cycle was resolved. Figure 4 shows the MTF plotted as a function of spatial frequency for 10,20,50 and 100 iterations of the restoration algorithm. Figure 5 shows the effect of the regularization algorithm on the MTF. Figure 6 shows the 50 % MTF value plotted as a function of iteration with and without regularization. The graph clearly shows that as the number of iterations is increased the Nyquist limit of 4.5 line pairs per millimetre is asymtopically approached. The regularized deconvolution is seen to approach the limit more slowly. It is noteworthy that even after a modest number of iterations the resolution is significantly improved. Figure 6 shows that a 50 % increase in resolution is possible after only 20 iterations for both cases. Although Figures 4 and 5 clearly show the improvement in resolution, they do not obviously show the limitation imposed by amplification of noise. In order to investigate this we applied the restoration algorithm to one of the pinholes *not* used in the PSF measurement. A line profile is shown in Fig 7 for the original and after 20 and 50 iterations. The full width at half maximum (FWHM) for the original image was measured as 2.59 pixel. The SNR, calculated as the peak intensity divided by the standard deviation of the background noise was 20.9. After 20 iterations the FWHM has decreased by approximately 20 % to 2.11 pixel and the SNR is 20.5. After 50 iterations the FWHM is 2.09 pixel and the SNR is has decreased to 18.3 due to noise amplification. These results indicate that amplification of noise becomes a limiting factor as the number of iterations is increased. But with the regularized deconvolution the FWHM after 20 iterations is 2.30 however the SNR is 62.2 due to a much reduced noise level. The FWHM after 50 iterations is 2.12 and the SNR is 32.1. The line profiles for the regularized deconvolution are shown in Fig 8.

5. CONCLUSION AND FURTHER WORK

We have shown that when the instrumental PSF is accurately measured, the maximum likelihood image restoration is capable of improving resolution in digital mammography images by up to a factor of 2. This will significantly improve the identification of high frequency artifacts which would otherwise be lost in scattering induced fog. The ability to compensate for scattering may allow for the removal for the anti-scattering grid with a corresponding decrease in exposure time. We have also shown that regularization of the iterative deconvolution algorithm by application of the wavelet shrinkage technique to the residual between iterations is capable of increasing the signal to noise ratio in the restored image. Furthermore we have identified several promising areas of future work. We are currently investigating oversampling and sub-pixel registration of the image in order to reduce the effective pixel size. Preliminary work has shown that this method produces a more accurate PSF with a corresponding increase in resolution. We are also interested in simulating scattering within the breast using a Monte-Carlo algorithm in order to investigate the effect of scatter on the PSF - in particular to determine to what extent the PSF is depth dependent. The large image size involved in this work and the nature of the algorithm suggest that parallelization of the restoration algorithm should be pursued.

ACKNOWLEDGMENTS

We gratefully acknowledge the support of Enterprise Ireland, the Irish Research and Development Agency for their continuing support of this program. The Western Health Board is thanked for their kind support.

We would also like to acknowledge the developers of the IRAF[16] image processing package. The IRAF STSDAS (version 2.0) LUCY implementation of the restoration algorithm described in Section 2.1 was used in our experiments.

REFERENCES

1. R. A. Smith, "Epidemiology of breast cancer," in *Syllabus: 79th Scientific Assembly of the Radiological Society of North America*, pp. 21–33, 1993.
2. T. Holland, "So-called interval cancers of the breast: pathologic and radiographic analysis," *Cancer* **49**, pp. 2527–2533, 1982.
3. E. Hall, "A survey of pre-processing and feature extraction techniques for radiographic images," *IEEE Trans. Computing* **C**, pp. 1032–1044, September 1971.
4. E. D. Parades, "Radiographic breast anatomy: radiologic signs of breast cancer," in *Syllabus: 79th Scientific Assembly of the Radiological Society of North America*, pp. 35–46, 1993.
5. E. Sickles, "Mammographic detectability of breast microcalcifications," *AJR* (139), pp. 913–918, 1982.
6. B. B. Muir, "Microcalcification and its relationship to cancer of the breast: experience in a screening clinic," *Clinical Radiology* (149), pp. 193–200, 1983.
7. E. A. Sickles, "Mammographic features of 300 consecutive non palpable breast cancers.," *AJR* (146), pp. 662–663, 1986.
8. H. E. Johns, *The Physics of Radiology*, Charles C Thomas Pty Ltd, 4th ed., February 1983.
9. P.Abbott and A.Shearer, "Scatter correction in digital mammograph by deconvolution," 1999. In prepararation.
10. J. Henry, "Solid state x-ray detectors for digital mammography," in *SPIE Medical Imaging*, 1995.
11. L. Lucy, "An iterative technique for the rectification of observed distributions," *Astronomical Journal* (79), pp. 745–, 1974.
12. J.L.Starck and F. Murtagh, "Image restoration with noise suppresion using the wavelet transform," *Astronomy and Astrophysics* **288**, pp. 343–348.
13. I. Daubechies, *Ten lectures on wavelets*, SIAM, 1992.
14. D. L. Donoho, "De-noising by soft-thresholding," *IEEE Transactions on Information Theory* **41**, pp. 613–, 1995.
15. R. Butler, "Triffid photometry of globular cluster cores -i," *MNRAS* (296), pp. 379–391, 1998.
16. *Image Reduction and Analysis Facility.* http://star-www.rl.ac.uk/iraf/web/iraf-homepage.html.

Figure 2. TORMAX Breast Phantom

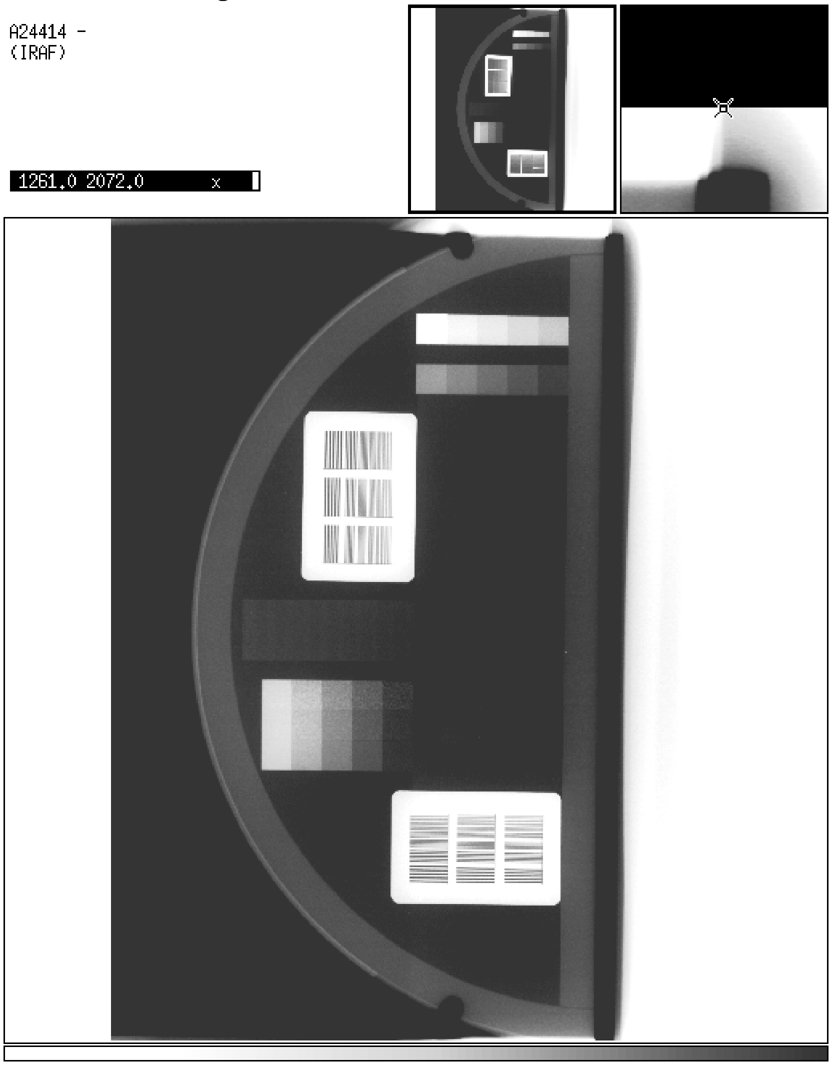

A24414 - SAOimage mammo@zag.ucg.ie Wed Apr 29 19:02:47 1998

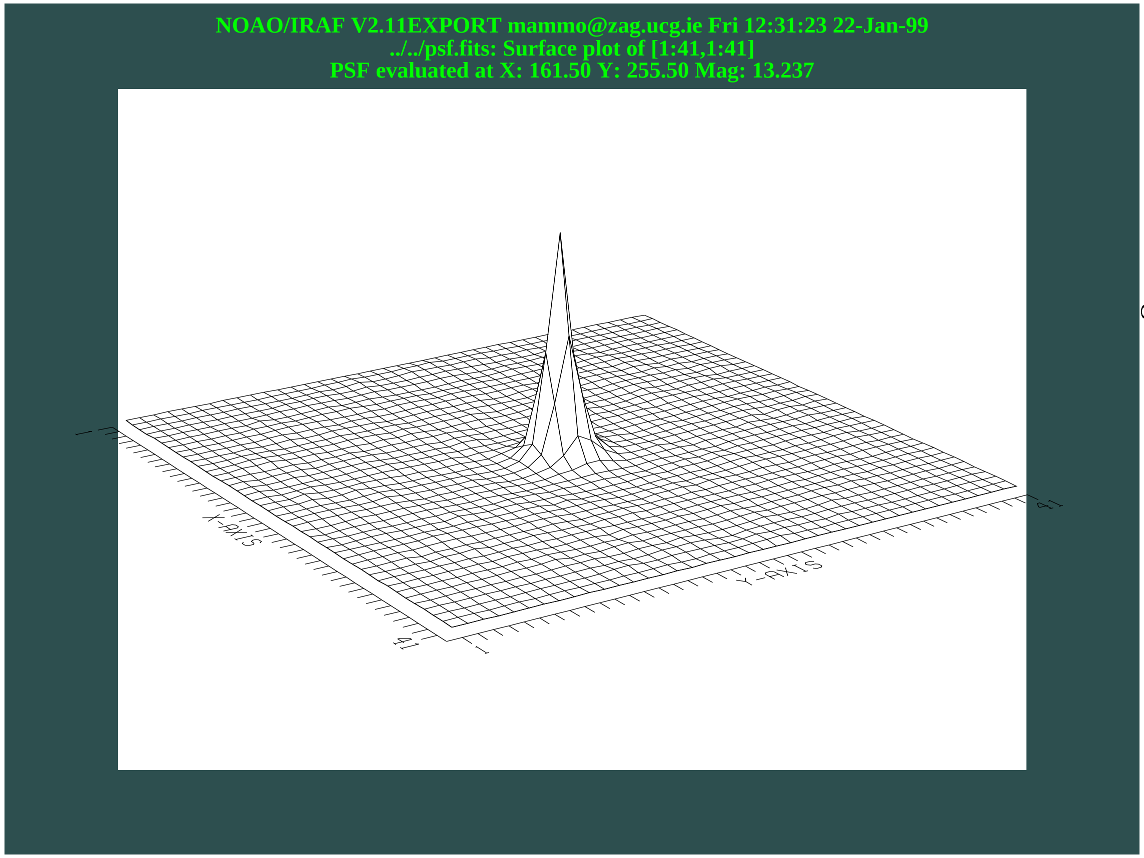

Figure 3. Measured PSF

Figure 4. Modulation transfer function for 10,20,50,100 iterations

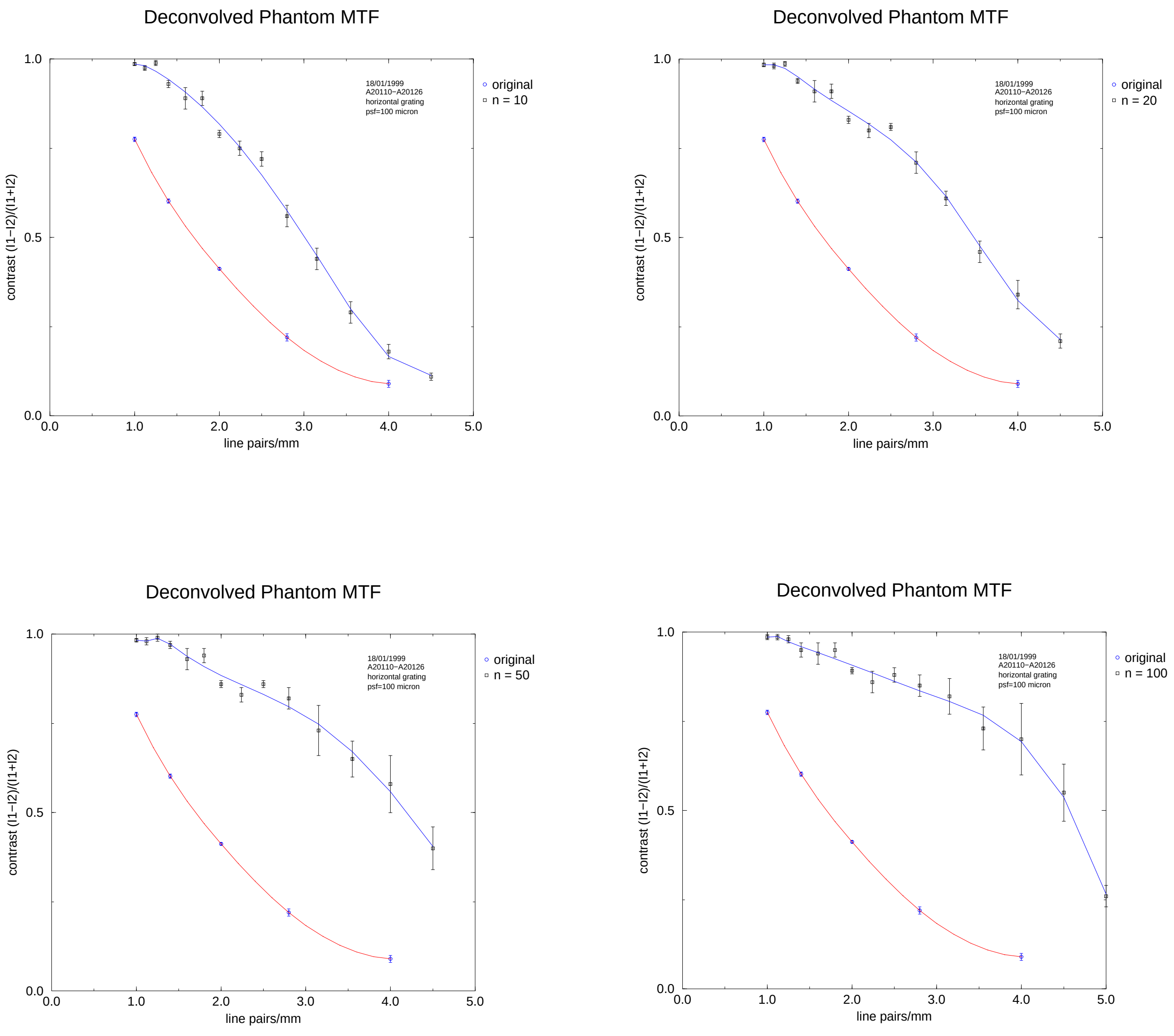

Figure 5. Modulation transfer function for 10,20,50,100 iterations with regularization

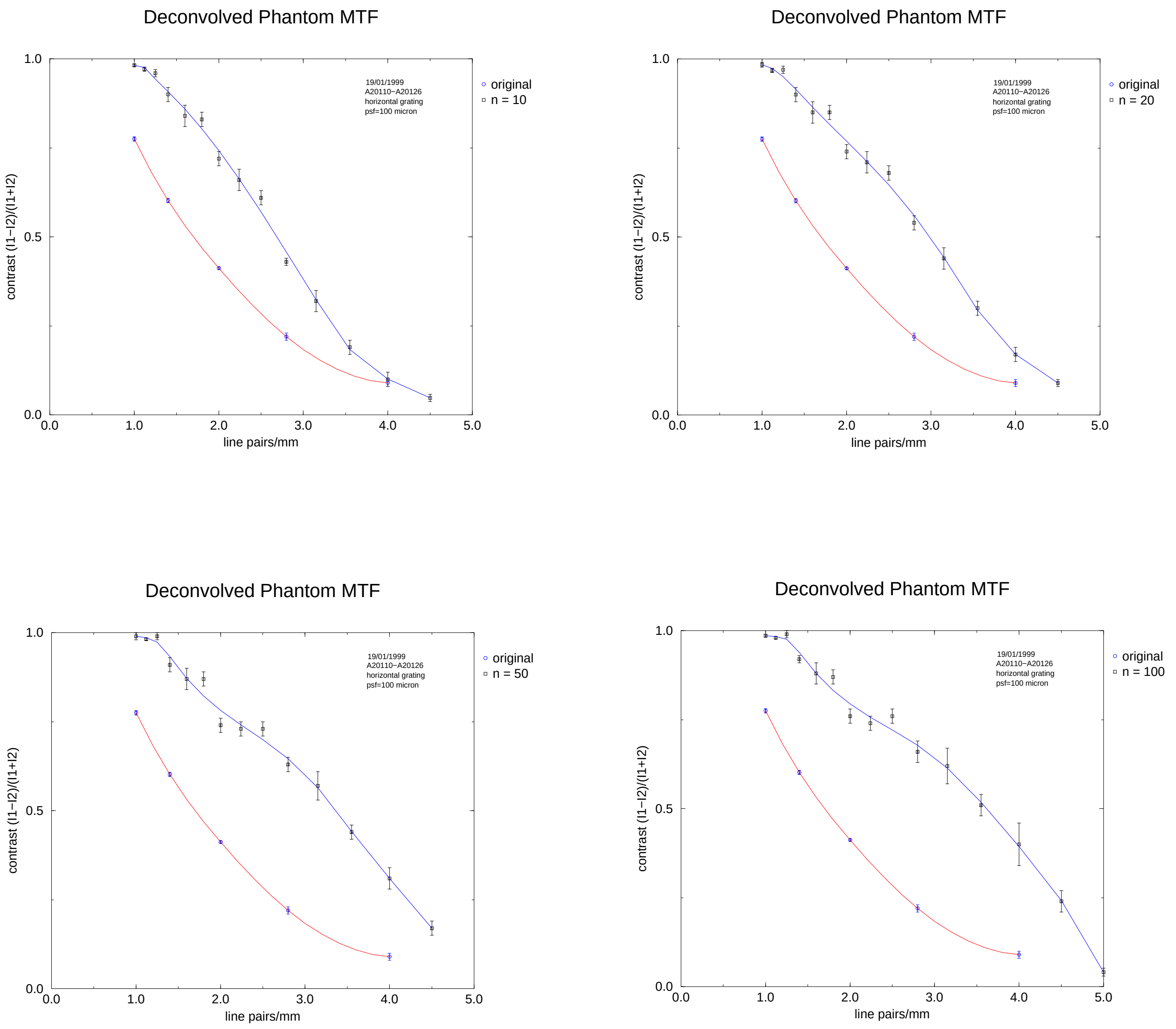

Figure 6. 50 percent MTF Level as a function of iteration for original and regularized deconvolution

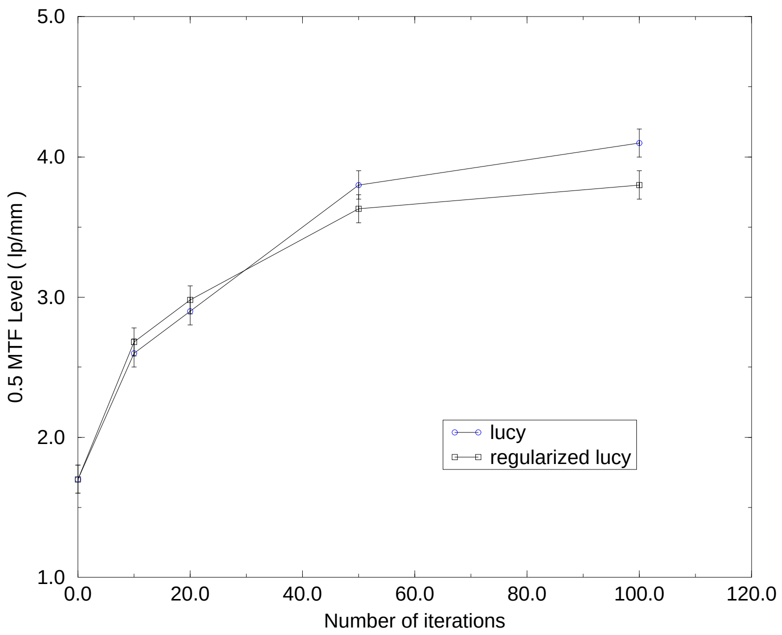

Figure 7. Original and deconvolved (n=20 and n=50) pinhole.

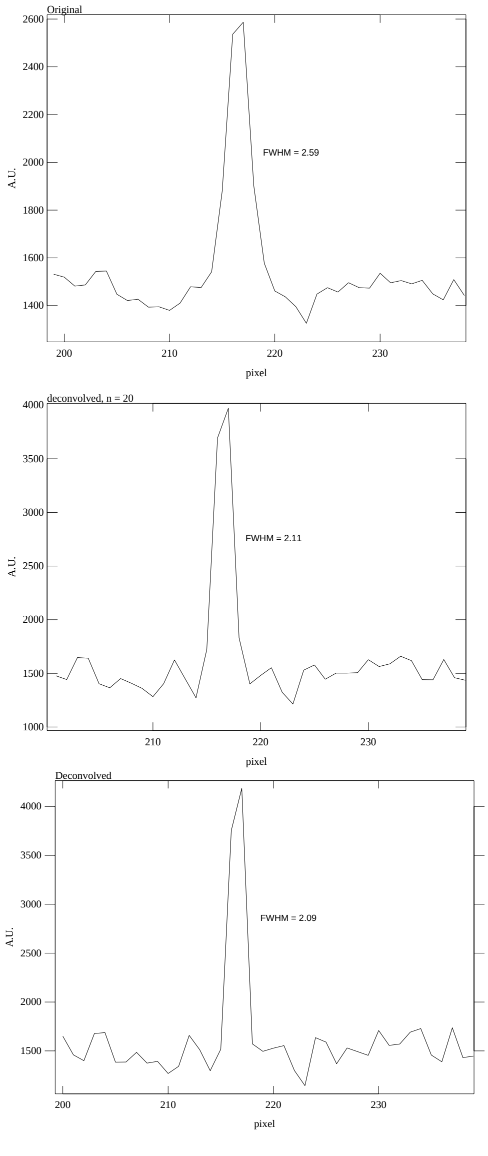

Figure 8. Original and deconvolved (n=20 and n=50) pinhole with regularization